The physics mechanisms of the weakly coherent mode in the Alcator C-Mod Tokamak

Z. X. Liu, X. Q. Xu, X. Gao, A. E. Hubbard, J. W. Hughes, J. R. Walk, C. Theiler, T. Y. Xia, S. G. Baek, T. Golfinopoulos, D. Whyte, T. Zhang, and J. G. Li

Citation: Physics of Plasmas **23**, 120703 (2016); doi: 10.1063/1.4972088
View online: http://dx.doi.org/10.1063/1.4972088
View Table of Contents: http://aip.scitation.org/toc/php/23/12
Published by the American Institute of Physics

The physics mechanisms of the weakly coherent mode in the Alcator C-Mod Tokamak

Z. X. Liu,[1,2,a)] X. Q. Xu,[2] X. Gao,[1] A. E. Hubbard,[3] J. W. Hughes,[3] J. R. Walk,[3] C. Theiler,[3] T. Y. Xia,[1,2] S. G. Baek,[3] T. Golfinopoulos,[3] D. Whyte,[3] T. Zhang,[1] and J. G. Li[1]
[1]*Institute of Plasma Physics, Chinese Academy of Sciences, Hefei, Anhui 230031, China*
[2]*Lawrence Livermore National Laboratory, Livermore, California 94550, USA*
[3]*MIT Plasma Science and Fusion Center, Cambridge, Massachusetts 02139, USA*

(Received 15 August 2016; accepted 27 November 2016; published online 8 December 2016)

The weakly coherent mode (WCM) in I-mode has been studied by a six-field two-fluid model based on the Braginskii equations under the BOUT++ framework for the first time. The calculations indicate that a tokamak pedestal exhibiting a WCM is linearly unstable to drift Alfven wave (DAW) instabilities and the resistive ballooning mode. The nonlinear simulation shows promising agreement with the experimental measurements of the WCM. The shape of the density spectral and location of the spectral peak of the dominant toroidal number mode $n = 20$ agrees with the experimental data from reflectometry. The simulated mode propagates in electron diamagnetic direction is consistent with the results from the magnetic probes in the laboratory frame, a large ratio of particle to heat diffusivity is consistent with the distinctive experimental feature of I-mode, and the value of the simulated χ_e at the edge is in the range of experimental errors of χ_{eff} from the experiment. The prediction of the WCM shows that free energy is mainly provided by the electron pressure gradient, which gives guidance for pursuing future I-mode studies. *Published by AIP Publishing.* [http://dx.doi.org/10.1063/1.4972088]

I-mode,[1,2] explored on the Alcator C-Mod tokamak[3] as well as ASDEX Upgrade[4] and DIII-D,[5] is a promising alternative regime for ITER and reactor-scale operation, characterized by its apparent decoupling of energy and particle transport, which results in good energy confinement without impurity accumulation. The regime is naturally stable to Edge Localized Modes. I-mode is accompanied by a reduction in edge turbulence in the mid-frequency range of 50–200 kHz and usually exhibits a higher-frequency (about 200–400 kHz) fluctuation, dubbed the "weakly-coherent mode" (WCM).[1,6–8] The WCM is well characterized experimentally on C-Mod, with density, temperature, and magnetic fluctuations visible on multiple diagnostics.[7–9] The density fluctuation is typically stronger by a factor of 5–10.[8] Recent MHD calculations using the ELITE code[10] indicate that I-mode pedestals are strongly stable to edge peeling-ballooning instabilities and ideal ballooning mode calculations suggest stability to the kinetic ballooning mode (KBM). Cross-bispectral measurements of the spectral transfer of density fluctuations showed that the geodesic-acoustic mode (GAM) is responsible for the broadened frequency structure of the WCM.[8] But the underlying physics basis of the WCM has been poorly understood.

The three-field model under the BOUT++ framework[11,12] has successfully simulated the nonlinear crash phase of ELMs,[13,14] which is mainly driven by the Peeling-Ballooning mode, and also implied quasi-coherent mode (QCM) in the Enhanced D_α (EDA) H-mode is driven by resistive Ballooning mode.[15] In this paper, the electromagnetic six-field two-fluid model, including more physics such as ion acoustic waves, thermal conductivities, Hall effect, compressibility, and electron-ion friction, has been used to simulate the WCM and elucidate the nature and underlying physics mechanisms. The equations used here are given explicitly in Ref. 14.

In this letter, the equilibrium of C-Mod I-mode discharge No. 1120907032 is used for the simulations. The discharge parameters are $I_P = 1.1$MA, $B_T = 5.8$ T, average additional heating power $P_{ICRF} = 5$ MW. The geometry of this discharge is lower single-null with the $B \times \nabla B$ drift directed away from the active X-point. The time evolution of the mode frequency spectrum is shown in Fig. 1(a). The WCM appears with a frequency centered on 350 kHz following the transition from the "low confinement" (L-mode) to the I-mode at 0.75 s. The toroidal mode number of the WCM is from $n = 15$ to 25 propagating in the electron diamagnetic drift direction in the laboratory frame, as diagnosed by magnetic probes, and the effective average of χ_i (ion thermal diffusivity) and χ_e (electron thermal diffusivity) is around 0.2 m^2/s measured from a power balance across the pedestal region ($r/a = 0.95$–1) as shown in Figs. 1(b) and 1(c). We use quasi-neutrality ($n_e = n_i$) and flat profiles in the SOL region as "model assumptions," so the profiles in the simulation (solid red curves in Fig. 2) are a little different from the experimental data (dashed blue curve in Fig. 2). The number of grid points in each direction is $n_\Psi = 260$, $n_\theta = 64$, and $n_\zeta = 64$, where Ψ, θ, and ζ are the radial, poloidal, and toroidal coordinates. The nonlinear simulation results are subjected to the following assumptions. The simulation is gradient driven. The net equilibrium zonal flow is set to be zero, so the interaction of the WCM with GAMs is not included. A fixed radial electric potential (E_r) profile has been used that makes the system in the nonlinear simulation

a)Author to whom correspondence should be addressed. Electronic mail: zxliu316@ipp.ac.cn

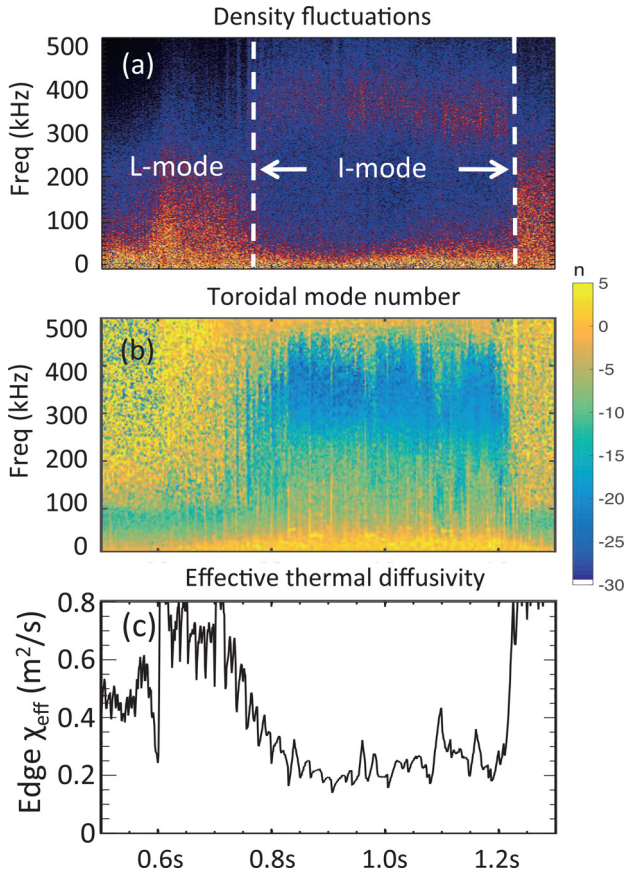

FIG. 1. Experimental data: (a) Spectrum of the density fluctuation mode diagnosed from reflectometry at $\psi = 0.988$. (b) Toroidal numbers of the modes calculated by data from magnetic probes. (c) Effective thermal diffusivity χ_{eff} from a power balance across the pedestal region (r/a from 0.95 to 1) and assuming power is split between ion and electron channels.

not self-consistent. Applying new BOUT++ capability including impurity species, the real profile in the SOL region, and GAM will be the future work.

Linear simulations with ideal MHD terms (black dashed curve with crosses in Fig. 3) show zero growth rates indicating

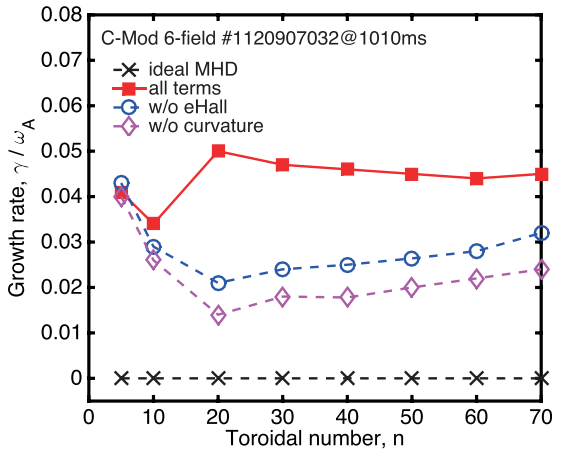

FIG. 3. Growth rate vs toroidal mode number in linear BOUT++ simulations. The black dashed curve with crosses is the case with ideal MHD; red solid curve with squares is the case with all terms in the six-field model; blue dashed curve with circles is the case without the eHall term; and the pink dashed curve with diamonds is the case without the curvature term.

that there is no Peeling-Ballooning mode, which is consistent with the absence of ELMs in the I-mode phase. When all terms in the six-field model are considered, a strong instability (solid red curve with square in Fig. 3) exists at $n \geq 20$. From testing of the terms in the six-field model separately, we found that the eHall (electron Hall effects) term and the curvature term are the most important contributions. Parallel conductivity normalized by the diamagnetic frequency $\omega_* = kT_{e0}/L_N$[16] has been scanned and used to identify the mode. The scan with all terms shows a complex behavior as shown in Fig. 4, but the scan with curvature only shows good agreement with the theory of the resistive ballooning mode[17] at $\sigma_\parallel/\omega_* > 0.002$. The scan without curvature has a peak at $\sigma_\parallel/\omega_* = 2$, which is similar to the trend of the theory of the collisional drift wave[19] (it might be modified by other terms). The propagation direction of the frequency in the plasma frames ($E_r = 0$) is another way to identify the mode. Figure 5(a) shows that mode without the curvature term propagates in the electron diamagnetic drift

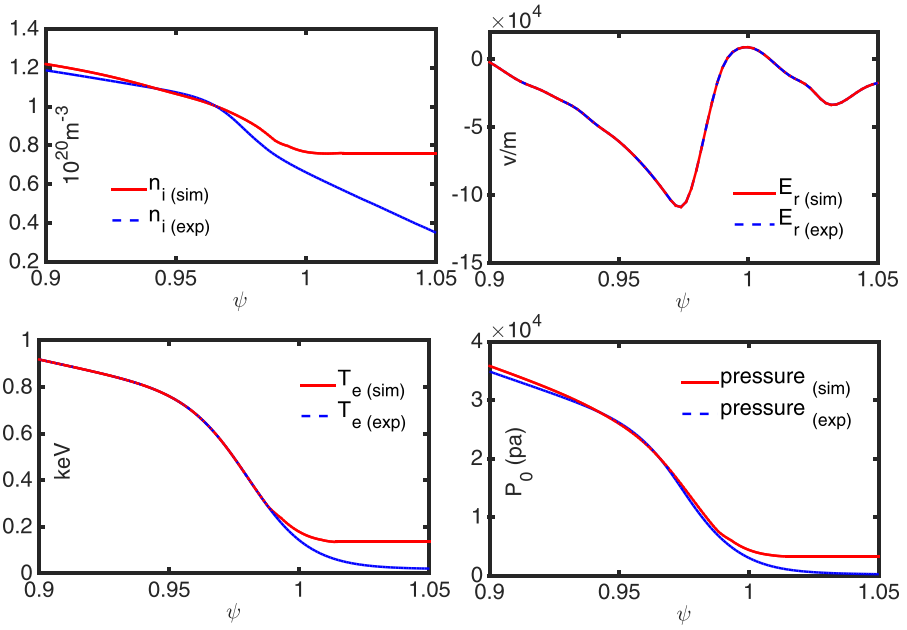

FIG. 2. Profiles in the simulation. Solid red curves are the profiles in the simulation. The dashed blue curves of n_i, T_e, *Pressure* are the profiles from kinetic EFIT based on the experimental data, and the dashed blue curve of Er is the experimental data obtained with CXRS[18] using a mid-plane gas puff as a neutral source.

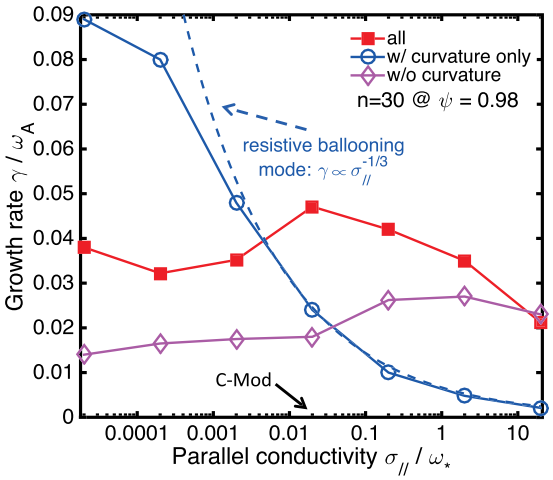

FIG. 4. Growth rate vs parallel conductivity. Red solid curve with squares is the case with all terms in the six-field model; blue solid curve with circles is the case with the curvature term only; and pink dashed curve with diamonds is the case without the curvature term.

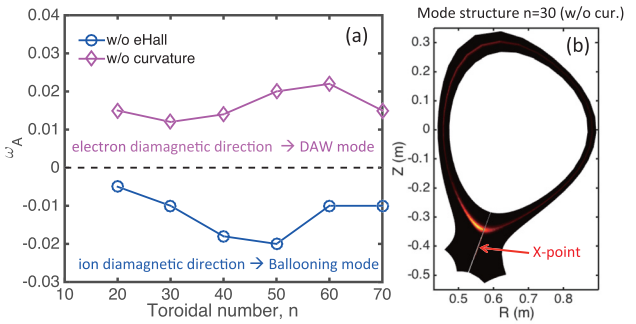

FIG. 5. (a) Frequency of the mode without eHall and without curvature; (b) Mode amplitude structure at $n=30$ without curvature in the linear simulation.

direction, which is in agreement with the drift Alfven wave (DAW) instability, while mode without the eHall term propagates in the ion diamagnetic direction, which is in agreement with the ballooning mode. In addition, the eigenmode at $n=30$ without curvature mainly peaks at the X-point and has a smaller component at the top of the machine as shown in Fig. 5(b), which is consistent with the eigenmode structure of the DAW instability described in the Gyrokinetic Toroidal Code (GTC) test.[20] Taken together, these tests indicate that the I-mode edge is linearly unstable to both the DAW instability and the resistive ballooning mode.

In order to compare the simulation results with the experimental measurements, nonlinear simulations have been performed. Figure 6 shows that the radial and poloidal locations of the peaks of the density fluctuations vary with mode number: $n=20$ peaks around $\psi=0.98$ while $n=15$ peaks around $\psi=0.94$ the outer midplane, in contrast to linear simulations. The different poloidal locations of the perturbation between the linear and nonlinear simulations should arise might due to the growth rate of the ballooning mode is stronger than growth rate of DAW implied from Fig. 3, but even the growth rate of DAW is dominant; Jingfei Ma's Ph. D. thesis[21] also provided a possible explanation that in addition to the anomalous radial heat transport at the top and X-point, where drift-Alfven modes peak in the linear stage, strong poloidal heat transport appears, which transfer a large amount of energy to the outboard mid-plane. The energy is then transferred through the radial transport at the outboard mid-plane. The time evolution of the density fluctuation of the modes from $n=5$ to 35 at $\psi=0.98$ (outer mid-plane) is shown in Fig. 7(a), a contour plot of density fluctuation amplitude versus toroidal mode number n and time at the peak gradient position $\psi=0.98$ at the outer mid-plane. It is stated that in the nonlinear phase the most unstable mode changes from $n=30$ to $n=20$. Since all modes have on average zero growth rate in the saturated stage, it could

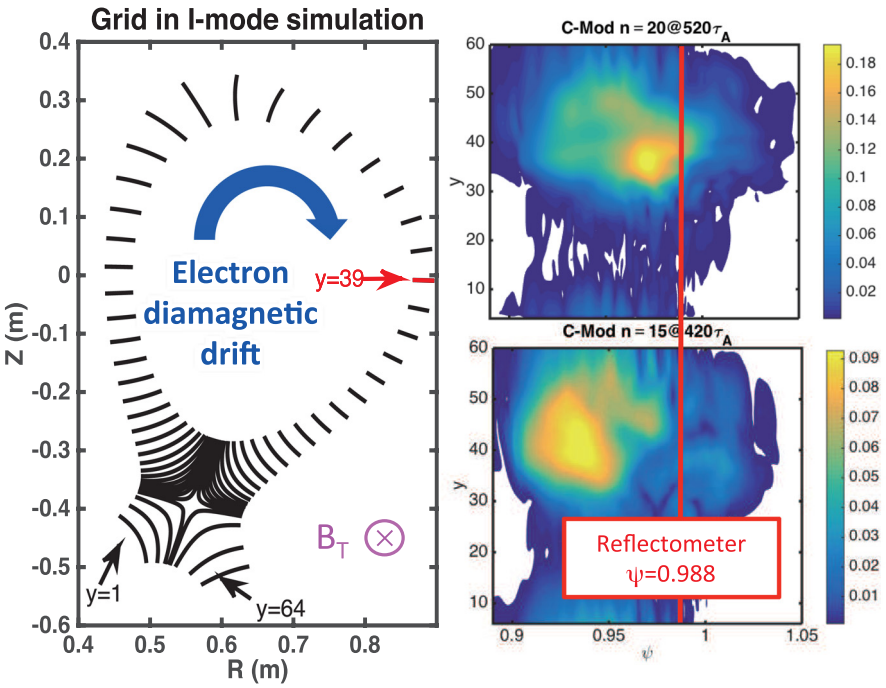

FIG. 6. Distribution of density fluctuations from the contribution of $n=15$ and $n=20$. The black curves in the left figure show the grid in the simulation, which is the y axis on other figures. The left figure also shows the direction of the electron diamagnetic drift and B_T. The position of the outer mid-plane is $y=39$.

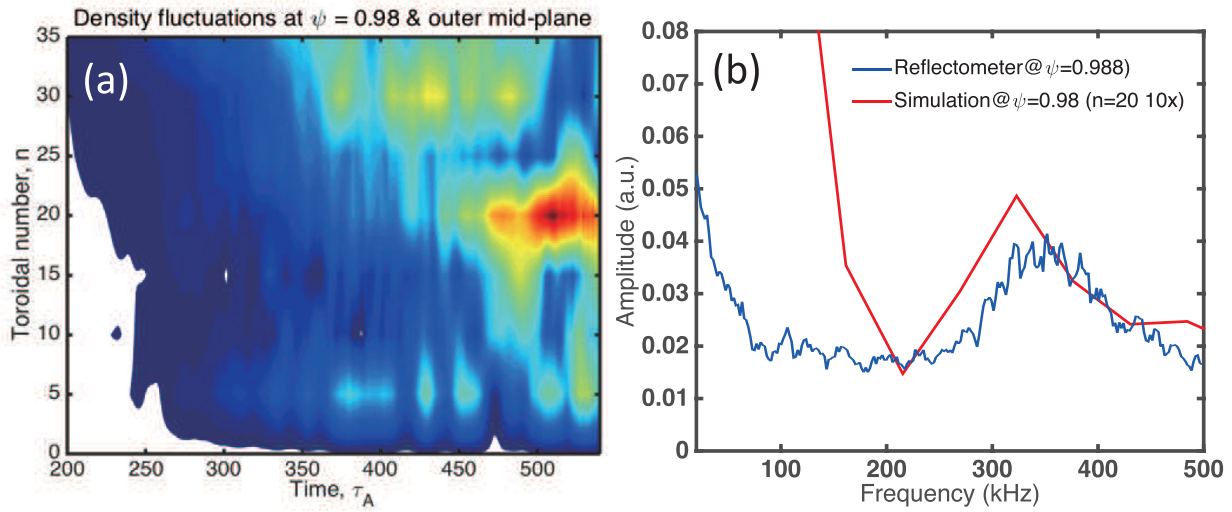

FIG. 7. (a) Time evolution ($200\tau_A$ ($\tau_A = 7.86 \times 10^{-5}$ ms) $\sim 540\tau_A$) of simulated density fluctuation amplitude of the modes from $n = 5$ to 35. (b) The red curve is the frequency spectrum of density fluctuation from the simulated mode $n = 20$ at $\psi = 0.98$ (outer mid-plane), and the blue curve is the frequency spectrum of the density fluctuation diagnosed by reflectometry at $\psi = 0.988$ (outer mid-plane).

be that the $n = 20$ mode has a lower growth rate than $n = 30$, but saturates at a higher level. Figure 7(b) shows the frequency spectrum of the $n = 20$ mode (red curve) at $\psi = 0.98$ and the frequency spectrum of the reflectometry[7,22] measurements (blue curve) at $\psi = 0.988$ (outer mid-plane). The two curves almost peak at the same frequency indicating rough agreement between the simulation and the experiment. Because the length of the nonlinear simulation is short, the spectral resolution from the simulation is very low and the error bar on frequency spectrum is 100% (single timeseries FFT). The direction of the predicted fluctuation is clockwise, aligned with the electron diamagnetic drift velocity, and the normalized density fluctuation from the simulation is about 10 times larger than the electron temperature fluctuation (details have been presented in Ref. 23). These features also agree with the experimental results.

Transport has been calculated from the nonlinear simulation. The solid curves with circles in Fig. 8 are the particle diffusivities D_e and D_i, and the solid curves are the thermal diffusivities χ_e and χ_i. The electron particle diffusivity is larger than the thermal, which is consistent with the key feature of I- mode, and the predicted χ_e roughly agree with the experimental χ_{eff} over $\psi = 0.95$ to 1(dashed black rectangle). However, ion channel seems to be a little complicated. Figure 9 shows that the fluctuation of the electron temperature is almost in phase with the electric potential from $425\tau_A$ to $525\tau_A$ ($\tau_A = 7.86 \times 10^{-5}$ ms), which means the electric potential fluctuation drives the electron temperature fluctuation.

The DAW is sensitive to the gradient of T_e,[21] but less sensitive to that of T_i. To clearly illustrate the correspondence, we have performed linear BOUT++ simulations for a scan of T_e and T_i ($T_{scan} = aT_{e,i}$) with the toroidal mode number $n = 30$, and with resistivity held fixed. The dashed black curve in Fig. 10 shows that the growth rate changes slightly with increasing T_e profile scale, if we use the calculated T_i profile ($T_i = P/n_e - T_e$) to keep the same pressure profile. The solid curves show that the growth rate has increased when the electron and ion increase separately, without enforcing self-consistence (no calculated T_i or T_e to offset the change). Increasing T_e or T_i separately will also increase the pressure gradient leading to higher growth rate from resistive ballooning mode, but the larger/faster increase

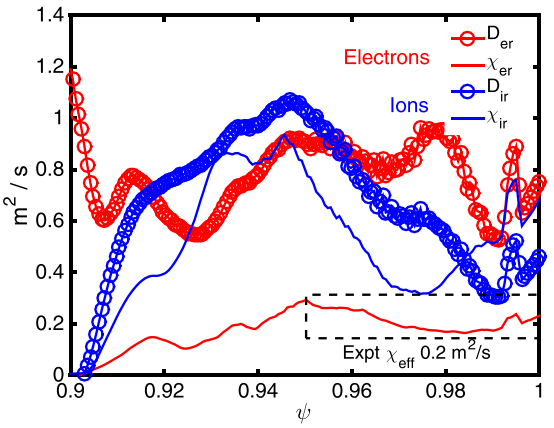

FIG. 8. Predicted particle and thermal diffusivities near the edge. The experimental range of values is indicated by the dashed black rectangle.

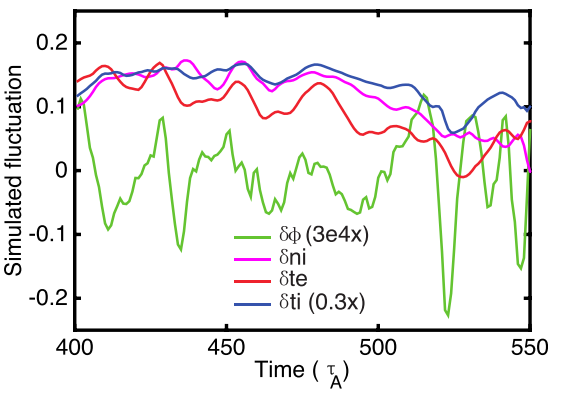

FIG. 9. Simulated fluctuations of electric potential, density, electron temperature, and ion temperature.

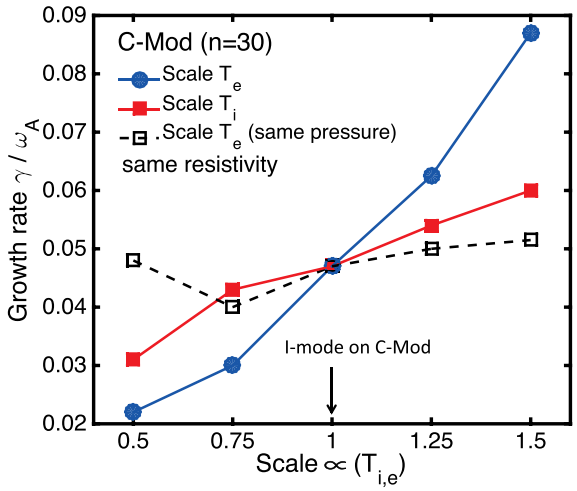

FIG. 10. Growth rate vs T_i and T_e with same resistivity.

of the growth rate in the T_e scan still indicates that the free energy for the mode is mainly from the electron pressure gradient, and increasing T_e at the edge should increase the WCM intensity. This result suggests that, in devices which have auxiliary heating predominately on ions and which have weak ion-electron coupling, additional electron heating may facilitate I-mode access. Note that C-Mod is primarily electron-heated and has strong ion-electron coupling, and routinely accesses I-mode.

In conclusion, BOUT++ simulations have been performed to elucidate the nature and underlying physics mechanisms of the WCM, which causes particle transport in I-mode pedestals of Alcator C-Mod. Key simulation results are that from the linear simulation, there is no ideal peeling-ballooning mode instability for the I-mode studied in agreement with Ref. 10; a strong instability exists at $n \geq 20$; I-mode edge with WCM is unstable to both the DAW instability and the resistive ballooning mode; the free energy for the WCM is mainly provided by the electron pressure gradient.

From the nonlinear simulation, the mode propagates in the electron diamagnetic direction; the predicted frequency of the $n = 20$ mode agrees with the measured WCM peaks around 350 kHz; the predicted χ_e agrees with the χ_{eff} from the experiment; and the predicted particle transport is larger than the predicted heat transport.

The authors wish to acknowledge Dr. Ben Dudson and Dr. M. V. Umansky for their contribution to the BOUT++ framework, Mr. E. Davis for useful physics discussions. This work was supported by the National Magnetic Confinement Fusion Program of China (Grant Nos. 2014GB106001 and 2014GB106003), and the National Natural Science Foundation of China (Grant Nos. 11021565, 11275234, 11405213, 11405215, 11405217, and 11422546), and was performed under the auspices of the U.S. DOE by LLNL under Contract No. DE-AC52-07NA27344, by Alcator C-Mod under Contract No. DE-FC02-99ER54512, and by PPPL under Contract No. DE-AC02-09CH11466.

[1]D. Whyte, A. Hubbard, J. Hughes, B. Lipschultz, J. Rice, E. Marmar, M. Greenwald, I. Cziegler, A. Dominguez, T. Golfinopoulos, N. Howard, L. Lin, R. McDermott, M. Porkolab, M. Reinke, J. Terry, N. Tsujii, S. Wolfe, S. Wukitch, Y. Lin, and the Alcator C-Mod Team, Nucl. Fusion **50**, 105005 (2010).
[2]R. M. McDermott, "Edge radial electric field studies via charge exchange recombination spectroscopy on the Alcator C-Mod tokamak," Ph.D. thesis (Massachusetts Institute of Technology, 2009).
[3]I. H. Hutchinson, R. Boivin, F. Bombarda, P. Bonoli, S. Fairfax, C. Fiore, J. Goetz, S. Golovato, R. Granetz, M. Greenwald, S. Horne, A. Hubbard, J. Irby, B. LaBombard, B. Lipschultz, E. Marmar, G. McCracken, M. Porkolab, J. Rice, J. Snipes, Y. Takase, J. Terry, S. Wolfe, C. Christensen, D. Garnier, M. Graf, H. Hsu, T. Luke, M. May, A. Niemczewski, G. Tinios, J. Schachter, and J. Urbahn, Physics of Plasmas **1**, 1511 (1994).
[4]P. Manz, P. Lauber, V. E. Nikolaeva, T. Happel, F. Ryter, G. Birkenmeier, A. Bogomolov, G. D. Conway, M. E. Manso, M. Maraschek, D. Prisiazhniuk, E. Viezzer, and the ASDEX Upgrade Team, Nucl. Fusion **55**, 083004 (2015).
[5]A. Marinoni, J. C. Rost, M. Porkolab, A. E. Hubbard, T. H. Osborne, A. E. White, D. G. Whyte, T. L. Rhodes, E. M. Davis, D. R. Ernst, K. H. Burrell, and the DIII-D Team, Nucl. Fusion **55**, 093019 (2015).
[6]A. E. Hubbard, D. G. Whyte, R. M. Churchill, I. Cziegler, A. Dominguez, T. Golfinopoulos, J. W. Hughes, J. E. Rice, I. Bespamyatnov, M. J. Greenwald, N. Howard, B. Lipschultz, E. S. Marmar, M. L. Reinke, W. L. Rowan, J. L. Terry, and Alcator C-Mod Group, Phys. Plasmas **18**, 056115 (2011).
[7]A. Dominguez, "Study of density fluctuations and particle transport at the edge of I-mode plasmas," Ph.D. thesis (Massachusetts Institute of Technology, 2012).
[8]I. Cziegler, P. H. Diamond, N. Fedorczak, P. Manz, G. R. Tynan, M. Xu, R. M. Churchill, A. E. Hubbard, B. Lipschultz, J. M. Sierchio, J. L. Terry, and C. Theiler, Phys. Plasmas **20**, 055904 (2013).
[9]A. White, P. Phillips, D. Whyte, A. Hubbard, C. Sung, J. Hughes, A. Dominguez, J. Terry, and I. Cziegler, Nucl. Fusion **51**, 113005 (2011).
[10]J. R. Walk, J. W. Hughes, A. E. Hubbard, J. L. Terry, D. G. Whyte, A. E. White, S. G. Baek, M. L. Reinke, C. Theiler, R. M. Churchill, J. E. Rice, P. B. Snyder, T. Osborne, A. Dominguez, and I. Cziegler, Phys. Plasmas **21**, 056103 (2014).
[11]X. Q. Xu, B. D. Dudson, P. B. Snyder, M. V. Umansky, and H. Wilson, Phys. Rev. Lett. **105**, 175005 (2010).
[12]X. Q. Xu, B. D. Dudson, P. B. Snyder, M. V. Umansky, H. Wilson, and T. Casper, Nucl. Fusion **51**, 103040 (2011).
[13]Z. X. Liu, X. Q. Xu, X. Gao, T. Y. Xia, I. Joseph, W. H. Meyer, S. C. Liu, G. S. Xu, L. M. Shao, S. Y. Ding, G. Q. Li, and J. G. Li, Phys. Plasmas **21**, 090705 (2014).
[14]T. Y. Xia, X. Q. Xu, and P. W. Xi, Nucl. Fusion **53**, 073009 (2013).
[15]E. M. Davis, M. Porkolab, J. W. Hughes, B. LaBombard, P. B. Snyder, and X. Q. Xu, 55th APS DPP Conference (2013).
[16]M. V. Umansky, R. H. Cohen, L. L. LoDestro, and X. Q. Xu, Contrib. Plasma Phys. **48**, 27 (2008).
[17]B. A. Carreras, L. Garcia, and P. H. Diamond, Phys. Fluids **30**, 1388 (1987).
[18]R. M. Churchill, C. Theiler, B. Lipschultz, R. Dux, T. Pütterich, E. Viezzer, Alcator C-Mod Team, and ASDEX Upgrade Team, Rev. Sci. Instrum. **84**, 093505 (2013).
[19]B. D. Dudson, M. V. Umansky, X. Q. Xu, P. B. Snyder, and H. R. Wilson, Comput. Phys. Commun. **180**, 1467–1480 (2009).
[20]D. P. Fulton, Z. Lin, I. Holod, and Y. Xiao, Phys. Plasmas **21**, 042110 (2014).
[21]J. F. Ma, "The macro- and micro-instabilities in the pedestal region of the Tokamak," Ph.D. thesis (The University of Texas, 2015).
[22]Y. Lin, J. Irby, P. Stek, I. Hutchinson, J. Snipes, R. Nazikian, and M. McCarthy, Rev. Sci. Instrum. **70**, 1078 (1999).
[23]Z. X. Liu, X. Q. Xu, X. Gao, A. E. Hubbard, J. W. Hughes, J. R. Walk, C. Theiler, T. Y. Xia, S. G. Baek, T. Golfinopoulos, D. Whyte, T. Zhang, E. Davis, and J. G. Li, 57th APS DPP Conference (2015), p. GO4.00005.